

# Study of InSb thin films grown on different substrates by the pulsed electrodeposition technique

Joginder Singh<sup>1</sup> · Rajaram Poolla<sup>1</sup>

Received: 31 December 2016 / Accepted: 25 May 2017 / Published online: 31 May 2017  
© Springer Science+Business Media New York 2017

**Abstract** Stoichiometric InSb thin films were prepared, on four different substrates, using a pulsed electrodeposition technique. The electrochemical bath used for the growth of InSb thin films was made up of a mixture of aqueous solutions of indium trichloride ( $\text{InCl}_3$ ), antimony trichloride ( $\text{SbCl}_3$ ), citric acid ( $\text{C}_6\text{H}_8\text{O}_7 \cdot \text{H}_2\text{O}$ ) and sodium citrate ( $\text{Na}_3\text{C}_6\text{H}_5\text{O}_7 \cdot 2\text{H}_2\text{O}$ ). Energy dispersive analysis of X rays along with X-ray diffraction (XRD) studies show that the elemental composition and crystallinity of thin films is strongly dependent on the ionic composition of the electrochemical bath. Stoichiometric InSb thin films can be grown on all the four substrates from the same bath, by properly selecting the composition of the bath. XRD studies show that the InSb thin films grown on all the four substrates have preferred orientation along the (111) plane. The presence of sharp Raman peaks of longitudinal optical phonon mode and transverse optical phonon mode in stoichiometric thin films confirm that they are of good crystallinity.

## 1 Introduction

Indium antimonide (InSb) is technologically an important semiconductor, having a direct band gap of 0.17 eV at 300 K and 0.23 eV at 80 K [1, 2]. It has the Zinc-blende crystal structure with a lattice constant and dielectric constant of 6.47 Å and 16.8. It is an excellent material for photonic crystal applications due its large dielectric constant and mechanical properties suitable for devices. Indium

antimonide semiconductor devices are capable of operating with voltages under 0.5 V, reducing their power requirements. Single crystal InSb and  $\text{InAs}_{1-x}\text{Sb}_x$  have been used as high mobility photodetectors in the Long Wavelength Infrared (LWIR) and Mid Wavelength Infrared (MWIR) [3].

InSb is one of the most studied binary III-V compounds with the hole mobility around ( $1250 \text{ cm}^2 \text{ V}^{-1} \text{ s}$ ) and electron mobility around ( $10,240 \text{ cm}^2 \text{ V}^{-1} \text{ s}$ ) at room temperature, the largest value of all semiconductors [4]. It is an important semiconductor in the field of infrared detectors, in the 3–5  $\mu\text{m}$  wavelength range [5, 6] and in electronic and optoelectronics devices due to its high electron mobility [7, 8]. It shows both n-type and p-type semi-conductivity. The indium rich thin films material exhibit p-type semi-conductivity and the antimony rich material exhibits n-type semi-conductivity. The n-type InSb thin films can also be used as biosensors to detect bacteria [9]. Owing to its unique properties, InSb is used as Hall sensors and magneto resistors [10, 11], speed-sensitive sensors [12, 13] and high speed transistors [7, 14]. InSb p-n junctions exhibit photovoltaic effect with infrared light and have 100% internal quantum efficiency [15]. It is also a source of terahertz radiation because it is a strong photo-Dember emitter.

Different physical and chemical techniques are available for the growth of micro- and nanostructured materials including InSb and other functional inorganic structures. The growth techniques include molecular beam epitaxy [16], flash evaporation [17], sputtering [18], vacuum evaporation [19], electro-spinning [20], chemical oxidative polymerization [21], and ultrasonic and chemical treatment approach, [22–30]. Electrodeposition is one of the best techniques for growing semiconductor thin films owing to its simple and inexpensive set-up, good reproducibility, high efficiency of material utilization, high growth rate and uniform deposition

✉ Rajaram Poolla  
prajaram@ymail.com

<sup>1</sup> School of Studies in Physics, Jiwaji University, Gwalior,  
MP 474011, India

over large substrates. Several others have reported the electrodeposition of InSb mainly from aqueous baths. Ortega and Herrero reported the electrodeposition of InSb thin films on Ti substrates, and showed that single phase growth occurred in a small range of voltages below  $-0.85$  V [31]. Machesney et al. electrodeposited InSb thin films on Ti, ITO and Cu substrates using the same electrolyte as [31] and while all films contained either In or Sb along with InSb, the stoichiometry varied with potential for Ti, but for ITO and Cu, it was mostly independent of potential [32]. Deposition from a single Indium salt bath on Sb substrates was reported by Kozlov et al. They studied the diffusion of In ions onto the Sb substrate and observed the formation of InSb compound after heat treatment of the substrate [33]. Fulop et al. reported the growth of InSb thin films of which the stoichiometry was found to depend primarily on the ratio of  $\text{InCl}_3$  to  $\text{SbCl}_3$  in the electrolyte, and to be less dependent on applied potential and pH [34]. Khan et al. prepared nanocrystalline InSb thin films that can be transferred to an industrial scale [35]. Hnida et al. [36], Das et al. [37] and Hnida et al. [38] have synthesized InSb nanowires using electrodeposition. Khan et al. also fabricated field effect transistors based on electrodeposited InSb nanowires thus demonstrating that device quality material can be obtained by this technique. Hsieh et al. electrodeposited stoichiometric InSb on a nickel (Ni) substrate in a room-temperature ionic liquid 1-butyl-1-methylpyrrolidinium dicyanamide (BMP-DCA), containing anhydrous  $\text{InCl}_3$  and  $\text{SbCl}_3$  with a molar concentration ratio of 1:1. The composition of the deposited InSb film was found to depend on both the applied potential and the deposition charge [39].

The present paper describes the growth and properties of InSb thin films obtained on four different substrates using a pulsed electrodeposition technique. Pulsed plating has several advantages over direct current plating including finer grain deposit, lower porosity, higher density, improved adhesion and hardness of deposit, better control of alloy composition and uniformity in thickness, etc. [40, 41]. To the best of our knowledge, this is the first report on the use of pulsed plating for the synthesis of InSb thin films. We have shown that by this technique, good quality stoichiometric InSb can be deposited on all the four substrates used. We have also found that semiconductor/InSb layers deposited by pulsed electrodeposition are more uniform and adhesive than dc electrodeposition.

## 2 Experimental details

### 2.1 Materials

Sodium citrate ( $\text{Na}_3\text{C}_6\text{H}_5\text{O}_7 \cdot 2\text{H}_2\text{O}$ ) and citric acid ( $\text{C}_6\text{H}_8\text{O}_7 \cdot \text{H}_2\text{O}$ ) from Fisher Scientific, Mumbai, India. Deionized water ( $\text{H}_2\text{O}$ ) from FAIRCHEM, India. Indium

chloride ( $\text{InCl}_3$ ) and antimony chloride ( $\text{SbCl}_3$ ) from CDH, New Delhi, India. All the chemicals were AR grade and were used as received without further purification.

### 2.2 Synthesis

InSb thin films were grown on copper, brass, stainless steel and fluorine doped tin oxide substrate using baths of four different compositions. The films were deposited by the pulsed electrodeposition technique using an EG&G PARC (VERSASTAT-II) computer controlled potentiostat. The composition of the bath was varied by changing the ionic antimony content from 0.02 to 0.05 M keeping the ionic indium content constant at 0.05 M. Increasing the  $\text{Sb}^{3+}$  content above 0.05 M in the electrochemical bath did not give good quality InSb films and therefore our work was limited to the following four bath compositions: In/Sb = 0.05/0.02, 0.05/0.03, 0.05/0.04 and 0.05/0.05 for baths B1 to B4.  $\text{SbCl}_3$  usually precipitates in water, so it was first dissolved in 0.3 M citric acid and then mixed with 0.05 M aqueous  $\text{InCl}_3$  solution. 0.2 molar sodium citrate ( $\text{C}_6\text{H}_5\text{Na}_3\text{O}_7$ ) was used as a complexing agent which brings the reduction potentials of In and Sb close to each other aiding in binary growth. Table 1 shows the weight in grams of each chemical used in the electrochemical baths. Each bath was made using 40 ml of DI water.

A carbon electrode was used as the counter electrode, and an Ag/AgCl electrode as the reference electrode. Copper, brass, stainless steel and fluorine doped tin oxide (FTO) substrates were used as the working electrodes on which the electrodeposition was obtained. The FTO layers used in this work were produced by the spray pyrolysis technique. The metal substrates were cleaned in dilute HCl after which they were cleaned ultrasonically in distilled water and acetone and then rinsed in distilled water. All the experiments were performed at room temperature. Each deposition was carried out for 15 min after adjusting the pH of the bath to 3.0. Cyclic voltammetry was used to analyze the bath and obtain the potential at which

**Table 1** Weight in grams of each chemical used in the electrochemical baths

Compounds	Wt. (in grams) For four different baths (B1 to B4)			
	B1	B2	B3	B4
$\text{InCl}_3$	0.2211	0.2211	0.2211	0.2211
$\text{SbCl}_3$	0.0912	0.1368	0.1842	0.2281
$\text{Na}_3\text{C}_6\text{H}_5\text{O}_7 \cdot 2\text{H}_2\text{O}$	0.256	0.256	0.256	0.256
$\text{C}_6\text{H}_8\text{O}_7 \cdot \text{H}_2\text{O}$	1.440	1.440	1.440	1.440

codeposition of In and Sb occurs. There is wide range of potentials ( $-0.8$  to  $-1.5$  V) at which codeposition is possible. In this paper, we present our work on the deposition of InSb at a potential of  $-1.3$  V using pulses of frequency 10 KHz. All the electrodeposited thin films were annealed at  $300$  °C in vacuum for 1 h.

### 3 Thin film characterization

The structural studies of the films were carried out on a Philips D 8 Advance X-ray diffractometer using Cu  $K_{\alpha}$  radiation of wavelength  $1.5406$  Å. The surface morphology and elemental compositional studies were investigated using a Carl Zeiss FE-SEM/EDAX Quanta 200 FEG microscope. The Raman study was carried out using a Raman spectrometer with a 514 nm LASER and a CCD detector. Electrical conductivity type was determined using the hot probe technique.

## 4 Results and discussion

### 4.1 Cyclic voltametric studies

Cyclic voltammetry was used to investigate the conditions appropriate for the electrodeposition of InSb. The successful deposition of semiconductors compounds is possible by adding suitable complexing agents or adjusting the ionic concentrations in the electrochemical bath. Prior to selecting the final bath compositions and deposition potential, the voltammograms (CV curves) of Indium and antimony baths as well as baths of various In/Sb ionic compositions were studied separately. Our studies indicate that the addition of sodium citrate is beneficial for the deposition of the semiconductor. The voltammetric studies show that pure In and Sb are deposited/reduced at and below  $-0.9$  and  $-0.6$  V, respectively. The addition of sodium citrate shifts the deposition potentials of Sb and In closer to each other. Figure 1 shows the voltammogram for a bath containing  $0.5$  M  $\text{InCl}_3$  and  $0.4$  M  $\text{SbCl}_3$  along with sodium citrate. Reduction of both ions now occurs at potentials below  $-1$  V (versus Ag/AgCl) as the voltammogram shows. The nucleation loop is clearly seen in the voltammogram indicating nucleation and growth of the deposit on the substrate [42, 43].

Information regarding the alloying of In and Sb is contained in the reverse scans of the voltammograms. Figure 2 shows the CV curves for electrolytes containing various Sb contents. Starting from a bath containing only indium ions, as the Sb ions are increased in steps, the stripping peak of indium shifts to more negative potentials and at the same time the peak height is reduced. The Sb stripping peak

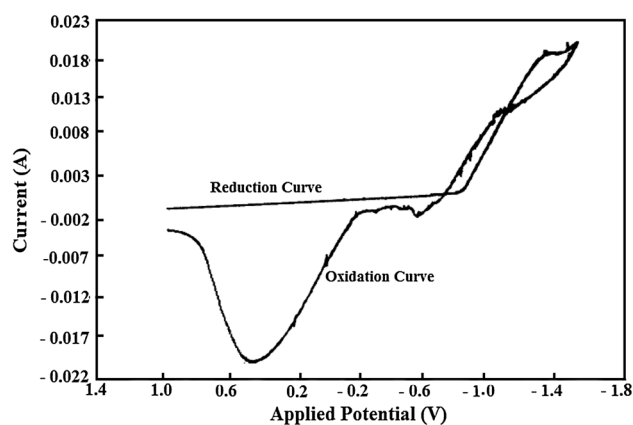


**Fig. 1** Cyclic voltammogram for a bath containing  $0.05$  M  $\text{InCl}_3$ ,  $0.04$  M  $\text{SbCl}_3$ ,  $0.30$  M sodium citrate and  $0.20$  M citric acid

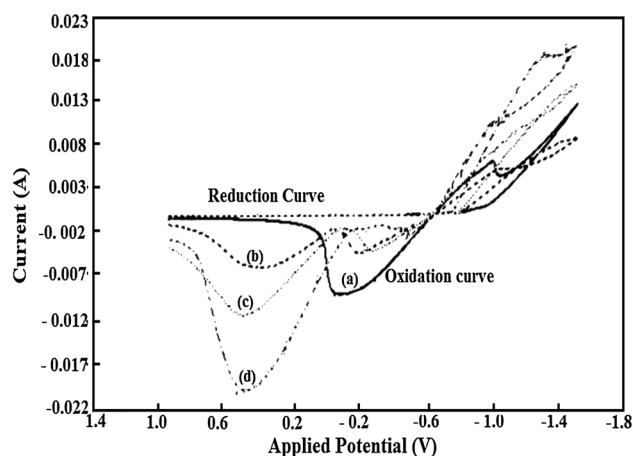


**Fig. 2** Cyclic voltammograms for baths containing **a**  $0.05$  M  $\text{InCl}_3$ ,  $0.02$  M  $\text{SbCl}_3$ ,  $0.30$  M sodium citrate,  $0.20$  M citric acid **b**  $0.05$  M  $\text{InCl}_3$ ,  $0.03$  M  $\text{SbCl}_3$ ,  $0.30$  M sodium citrate,  $0.20$  M citric acid **c**  $0.05$  M  $\text{InCl}_3$ ,  $0.04$  M  $\text{SbCl}_3$ ,  $0.30$  M sodium citrate,  $0.20$  M citric acid **d**  $0.05$  M  $\text{InCl}_3$ ,  $0.05$  M  $\text{SbCl}_3$ ,  $0.30$  M sodium citrate,  $0.20$  M citric acid

on the other hand becomes stronger as the Sb content is increased, but the shift in the position of the stripping peak is not very significant. These studies in conjunction with XRD and EDAX studies suggest that the shifting of the indium stripping peak towards negative potentials is associated with InSb compound formation.

### 4.2 X-ray diffraction studies

Figures 3 and 4 show the XRD patterns of as-grown and annealed stoichiometric InSb films, respectively, grown on the four different substrates at the potential  $-1.3$  V versus an Ag/AgCl electrode. The electrolytic bath was a mixture of aqueous solutions of  $0.05$  M  $\text{InCl}_3$ ,  $0.04$  M  $\text{SbCl}_3$ ,  $0.30$  M  $\text{C}_6\text{H}_8\text{O}_7 \cdot \text{H}_2\text{O}$  and  $0.20$  M  $\text{Na}_3\text{C}_6\text{H}_5\text{O}_7 \cdot 2\text{H}_2\text{O}$ . The

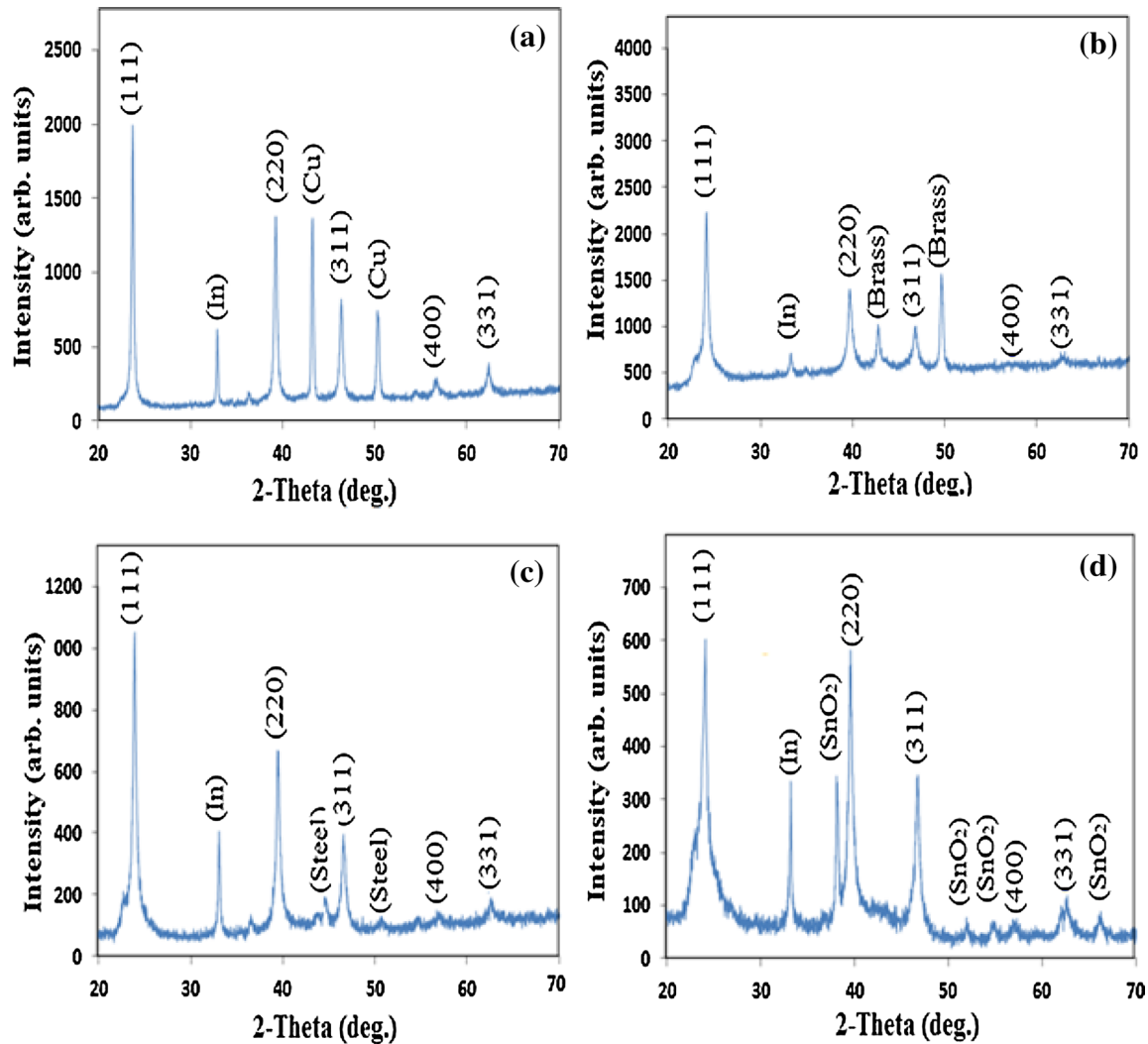


**Fig. 3** XRD patterns of as grown InSb thin films grown on **a** copper **b** brass **c** stainless steel and **d** fluorine doped tin oxide (FTO) substrates

diffraction data of InSb thin films grown on all the substrates, match with the standard diffraction data of InSb (JCPDS-ICDD No. 6-2008), showing the formation of zinc blende InSb thin films. The sharp diffraction peaks of as-grown and annealed samples deposited on the four different substrates reveal that the electrodeposited thin films are polycrystalline in nature. One can also see that the intensity of the diffraction peaks at  $2\theta=24^\circ$  is stronger than other diffraction peaks of the samples, and comparing the relative peak heights with those of the powder patterns shows that the InSb thin films grow preferentially along the (111) plane on all the four substrates. The diffractograms of as grown InSb thin films on the different substrates reveal the presence of minor additional peaks of In or Sb (or both) along with the main peaks of InSb. Annealing the films in vacuum at  $300^\circ\text{C}$ , reduces the intensity of these additional peaks in comparison to the InSb (111) peak as can be seen in the diffractograms of Fig. 4. For the brass substrate,

however, the lone minor peak of Indium, present for the as-grown film, is entirely eliminated on annealing the sample. Thus, the annealed InSb thin films grown on brass sheet substrates are single phase free from elemental In and Sb. Our X-ray diffraction studies are in agreement with studies on thin film InSb grown by other techniques [44, 45]. Most of the diffraction patterns exhibit a small shoulder for the (111) peak which is found to diminish on annealing. Such a shoulder has also been reported by Fulop et al. [34] who have attributed its presence to possible inhomogeneous stress in the samples.

The very sharp and narrow diffraction peaks confirm that the electrodeposited thin films are of good crystallinity. Figure 5 shows the XRD patterns of InSb thin films grown on brass sheet substrates, using baths of four different compositions, holding the indium content constant at 0.05 M. The XRD results show that the intensity of the diffraction peaks get stronger as the ionic content of Sb in the bath

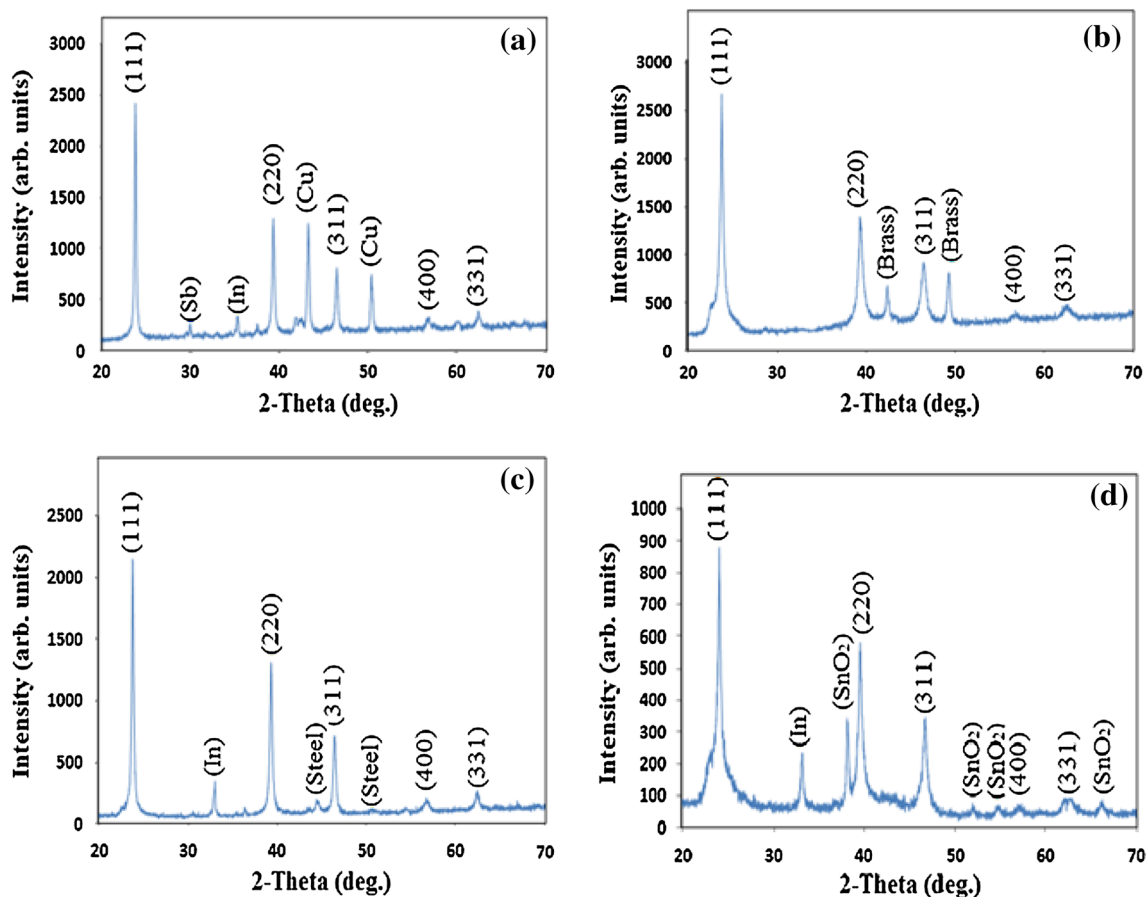


**Fig. 4** XRD patterns of annealed InSb thin films grown on **a** copper **b** brass **c** stainless steel and **d** fluorine doped tin oxide (FTO) substrate

increases from 0.02 to 0.04 M, the strongest peaks occurring for the Sb ionic composition 0.04 M. Compositional studies (Table 4), too, show that the bath containing 0.04 M  $\text{SbCl}_3$  and 0.05 M  $\text{InCl}_3$  gives InSb films having the best stoichiometry. This shows that best quality InSb is grown from a bath for which the In/Sb ionic ratio is 5/4. The lattice constant for this sample was found to be  $a=6.470 \text{ \AA}$  which is very close to the reported value. For films grown from baths with Sb ion content higher than 0.04 M Sb, the intensity of the XRD peaks is reduced and the stoichiometry is poor. A comparison of XRD data with standard data is shown in the Tables 2 and 3. The crystallite size was calculated using the Scherer formula [46]

$D = \frac{0.9\lambda}{\beta \cos\theta}$  where  $\lambda$  is wave length of X-rays ( $1.5406 \text{ \AA}$ ),  $\theta$  is the angle of incidence of X-rays,  $\beta$  is the full width at half maximum and 0.9 is the Scherer constant. The dislocation density  $\delta$  can be calculated using Williamson and Hallman's formula [47]

$$\delta = \frac{1}{D^2} \quad (2)$$

The micro strain of the thin films were also calculated using the equation [48]

$$e = \frac{\beta \cos\theta}{4} \quad (3)$$

The lattice parameter 'a' for the electrodeposited InSb thin films was calculated using the following equation [49]

$$d = \frac{a}{\sqrt{h^2 + k^2 + l^2}} \quad (4)$$

where h, k, l are the miller indices of the lattice planes and 'd' the inter planar spacing.

Table 2 shows the comparison of experimental d values for stoichiometric thin films deposited on various substrates with the standard d values of InSb. It can be seen that the d values for all the samples are close to the standard values with the maximum deviation around  $\pm 0.6\%$ . The best match occurs for the sample grown on brass substrates. Table 3 compares the d values for samples deposited on brass substrates using baths of



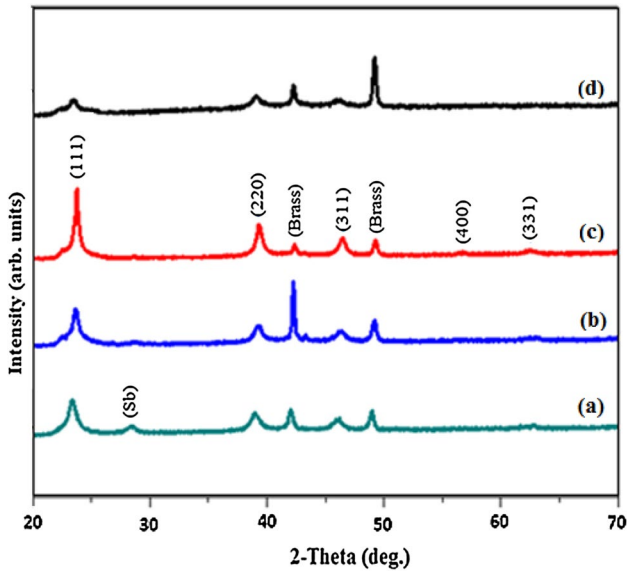


**Fig. 5** XRD of annealed InSb thin films grown on brass, from baths of composition *a* 0.05 M InCl<sub>3</sub>, 0.02 M SbCl<sub>3</sub>, 0.30 M sodium citrate, 0.20 M citric acid *b* 0.05 M InCl<sub>3</sub>, 0.03 M SbCl<sub>3</sub>, 0.30 M sodium citrate, 0.20 M citric acid *c* 0.05 M InCl<sub>3</sub>, 0.04 M SbCl<sub>3</sub>, 0.30 M sodium citrate, 0.20 M citric acid *d* 0.05 M InCl<sub>3</sub>, 0.05 M SbCl<sub>3</sub>, 0.30 M sodium citrate, 0.20 M citric acid

various compositions. As expected, the closest match with standard data occurs for the sample with the best stoichiometry.

The values of crystallite size, strain, dislocation density and lattice parameter for the films grown from baths of different composition are shown Table 4. From the table, we can see that the crystallite size is small for samples obtained from Sb deficient baths and increases with increase in Sb ionic concentration, reaching a maximum value for the sample with the best stoichiometry and grown from a bath containing an In/Sb ionic ratio of 5/4. The increase in crystallite size is accompanied by a decrease in the strain value and dislocation density in the films. The largest crystallite size, lowest micro strain and minimum dislocation density are observed for the films with the best stoichiometry and grown from the optimal bath.

### 4.3 Surface morphology and compositional studies

SEM studies of the samples show that the surface morphology and size of particles can be controlled by varying the composition of sodium citrate in the bath. Uniform growth does not occur without the addition of sodium citrate. When small amounts of sodium citrate are added to the bath, the films grown have cauliflower shaped particles or clusters (which increase in size as the quantity of sodium citrate is increased). However, as the concentration of sodium citrate is increased (to 0.256 g in 40 ml H<sub>2</sub>O), the morphology changes in such way that we now have a uniform growth of spherical particles. Further increase in the quantity of sodium citrate does not result in any further change in morphology, and so all samples investigated in

**Table 2** Comparison between observed and standard d values of thin films grown on different substrates

S. No.	2θ (deg.)	hkl planes	Copper sheet	Brass sheet	FTO	Steel sheet	Standard d values (Å)
			Observed d values (Å)	Observed d values (Å)	Observed d values (Å)	Observed d values (Å)	
1	24	(111)	3.73420	3.74240	3.71740	3.74438	3.74
2	39	(220)	2.28710	2.28880	2.27671	2.29101	2.290
3	46	(311)	1.95172	1.95378	1.94670	1.95409	1.953
4	56	(400)	1.62170	1.6241	1.61241	1.62158	1.62
5	62	(331)	1.48635	1.48440	1.48143	1.48630	1.480

**Table 3** Comparison between observed and standard d values of thin films grown on brass sheet substrates from baths of different compositions. (Note that the atomic percentages of the thin film samples are given in the table and not the bath compositions)

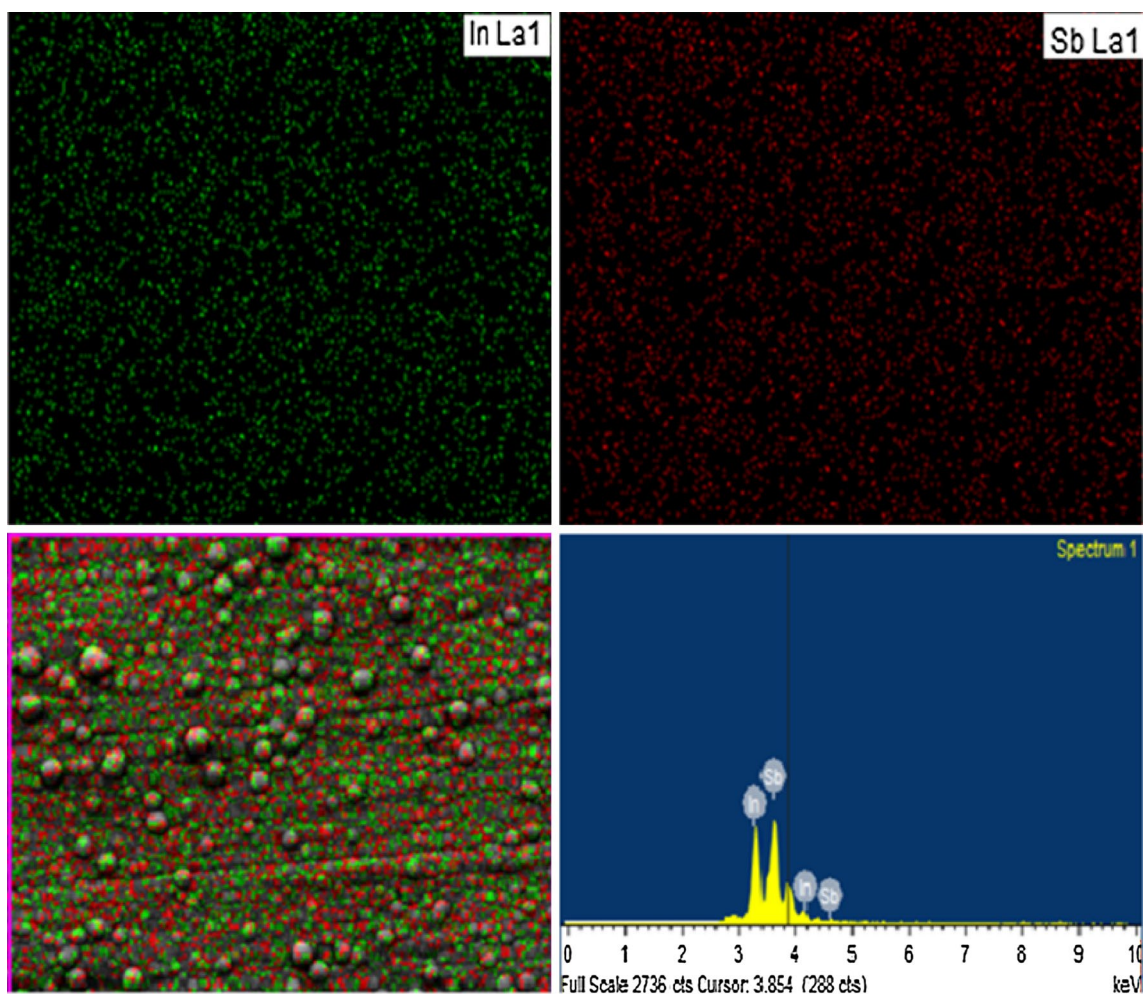
S. No.	2θ (deg.)	hkl planes	In: 64.07	In:56.04	In:49.62	In:44.13	Standard d values (Å)
			Sb:35.93 (Å)	Sb:43.96 (Å)	Sb:50.38 (Å)	Sb:55.87 (Å)	
1	24	(111)	3.71780	3.7291	3.74240	3.78194	3.74
2	39	(220)	2.27946	2.27105	2.28880	2.30204	2.290
3	46	(311)	1.94584	1.94741	1.95378	–	1.953
4	56	(400)	1.67960	–	1.62410	–	1.620
5	62	(331)	1.48635	1.41460	1.48440	–	1.480

**Table 4** Structural parameters from XRD for (111) plane grown on brass sheet substrate

Atomic ratios (In/Sb) in thin film (%)	Crystallite size (D) nm	Strain ( $\epsilon$ ) $\times 10^{-3}$ line <sup>-2</sup> m <sup>-4</sup>	Dislocation density $\delta \times 10^{14}$ line m <sup>-2</sup>	$d_{(111)}$ (Å)	Lattice parameter ( $a \times 10^{-10}$ m)
64.07/35.93	19.28	0.0091	0.00269	3.71780	6.43
56.04/43.96	24.24	0.0072	0.00170	3.7291	6.45
49.62/50.38	32.63	0.0054	0.00095	3.74240	6.47
44.13/ 55.87	16.97	0.0104	0.03472	3.78194	6.55

**Table 5** Molar ratios and atomic ratios of thin films grown on different substrates

Brass sheet		Copper sheet		FTO	
Molar ratios (In/Sb) in sol (M)	Atomic ratios (In/Sb) in thin film (%)	Molar ratios (In/Sb) in sol (M)	Atomic ratios (In/Sb) in thin film (%)	Molar ratios (In/Sb) in sol (M)	Atomic ratios (In/Sb) in thin film (%)
0.05/0.02	64.07/35.93	0.05/0.02	60.40/39.60	0.05/0.02	61.02/38.98
0.05/0.03	56.04/43.96	0.05/0.03	55.04/44.96	0.05/0.03	54.15/45.85
0.05/0.04	49.62/50.38	0.05/0.04	49.77/50.33	0.05/0.04	50.65/49.35

**Fig. 6** Elemental mapping images of EDS spectra for a stoichiometric InSb thin film grown on brass sheet substrate

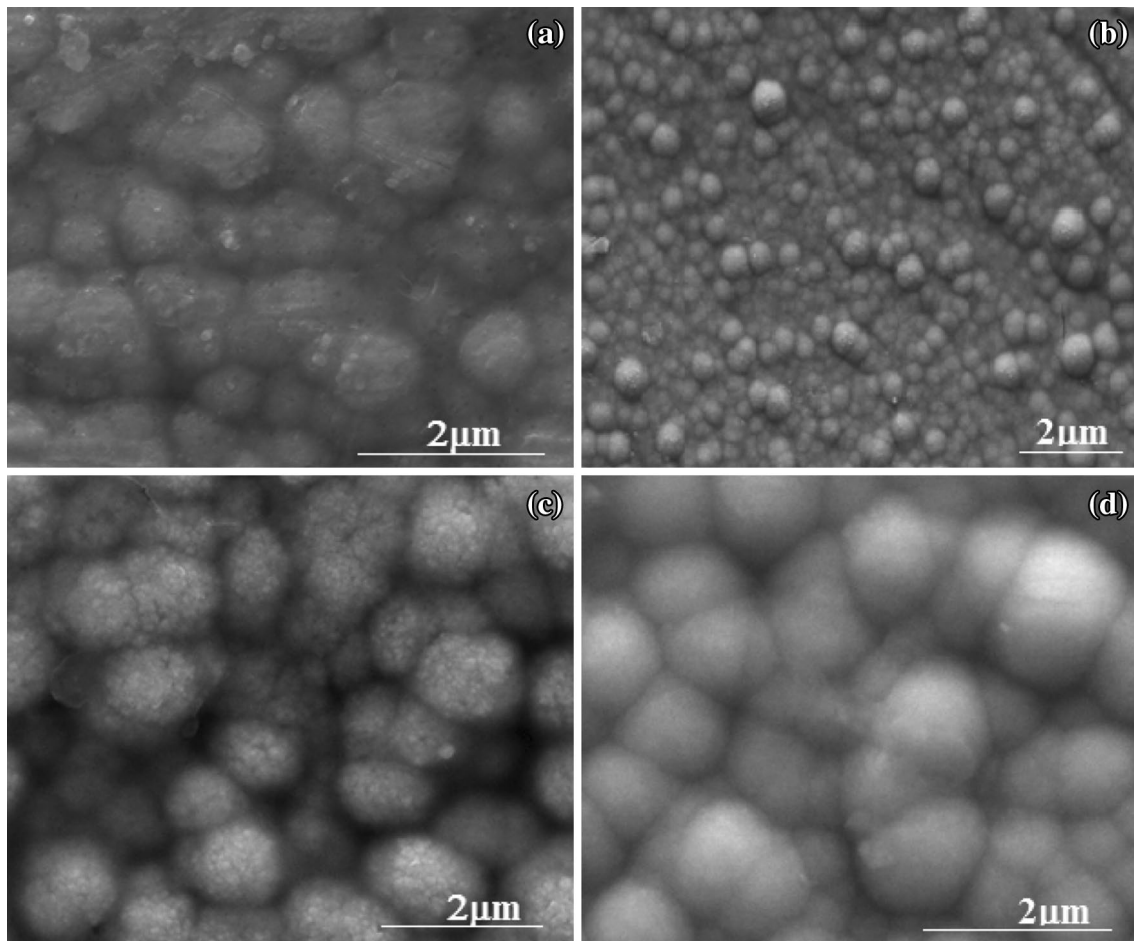


**Fig. 7** SEM micrographs of annealed InSb thin films grown on **a** copper **b** brass **c** stainless steel and **d** fluorine doped tin oxide (FTO) substrates

this work were grown from baths containing the above concentration of sodium citrate (0.256 g in 40 ml  $H_2O$ ).

EDAX studies conducted on the samples show that the composition of the films is strongly dependent on the molar ratios of In and Sb in the bath. Stoichiometric InSb thin films can be electrodeposited on all the four substrates, by properly selecting the bath composition. The EDAX data are summarized in Table 5 which shows the atomic In/Sb ratios for InSb thin films grown on different substrates using baths of different compositions. The results show that as the  $SbCl_3$  concentration in the electrolytic bath increases from 0.2 to 0.4 M, with the  $InCl_3$  concentration held constant at 0.05 M, the stoichiometry improves. Thin films obtained from the bath containing 0.05 M  $InCl_3$  and 0.04 M  $SbCl_3$  have the best stoichiometry. From the table, it can be seen that the films grown on all the four substrates, have very good stoichiometry provided they are grown from baths of above mentioned optimal composition. The XRD and SEM/EDAX results show that stoichiometric and good quality thin films free from extraneous peaks of In and Sb were obtained on brass sheet substrates. The EDS mapping

images for the stoichiometric InSb thin films on brass substrate are shown in Fig. 6. The images reveal that the elements In and Sb are distributed uniformly on the film surface.

Figure 7 shows the SEM images of electrodeposited stoichiometric thin films grown on different substrates. Figure 8 shows SEM images of electrodeposited InSb thin films grown on brass substrates, using baths of four different compositions. The SEM images in Figs. 7 and 8 show that the surfaces of the films are uniformly covered with spherical particles of size ranging from 0.1 to 0.5 micron. The surface morphology is almost similar on all the substrates although the size of the particles can be seen to be higher for tin oxide substrates. The SEM images in Fig. 8 show uniform growth and the morphology does not vary with electrolyte composition, except when the Sb content is higher than the optimal content or when the quantity of the complexing agent is low. It can be seen in Fig. 8d that the morphology is poor (consisting of cauliflower growth) when the Sb ionic content is high. The fact that the stoichiometry of the deposited InSb thin films is strongly



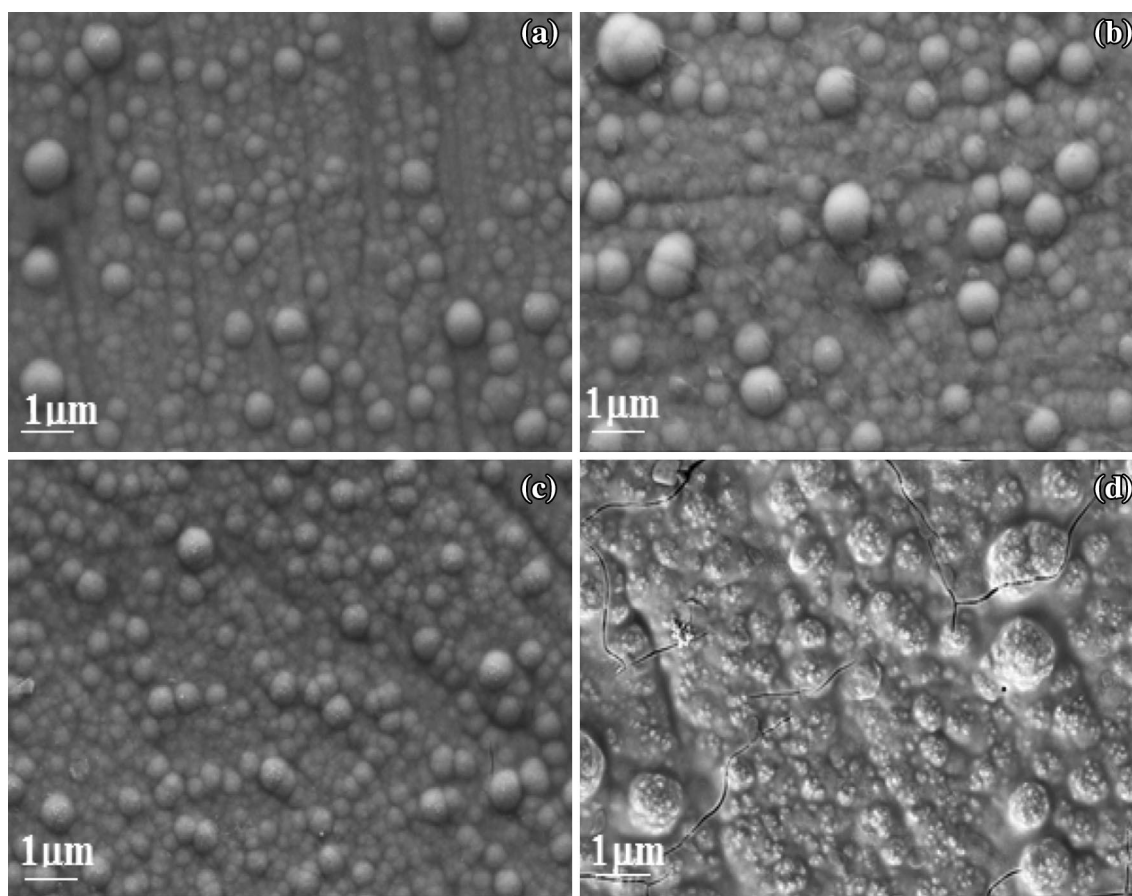


**Fig. 8** SEM micrographs of annealed InSb thin films grown on brass from baths of composition **a** 0.05 M  $\text{InCl}_3$ , 0.02 M  $\text{SbCl}_3$ , 0.30 M sodium citrate, 0.20 M citric acid **b** 0.05 M  $\text{InCl}_3$ , 0.03 M  $\text{SbCl}_3$ ,

0.30 M sodium citrate, 0.20 M citric acid **c** 0.05 M  $\text{InCl}_3$ , 0.04 M  $\text{SbCl}_3$ , 0.30 M sodium citrate, 0.20 M citric acid **d** 0.05 M  $\text{InCl}_3$ , 0.05 M  $\text{SbCl}_3$ , 0.30 M sodium citrate, 0.20 M citric acid

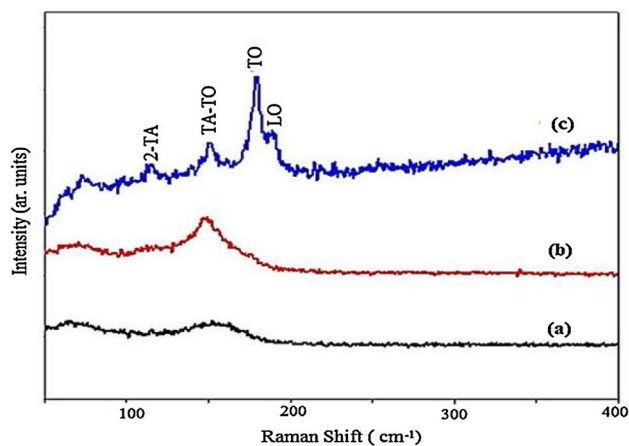


**Fig. 9** Raman spectra of annealed InSb thin films grown on brass, from baths of composition **a** 0.05 M  $\text{InCl}_3$ , 0.02 M  $\text{SbCl}_3$ , 0.30 M sodium citrate, 0.20 M citric acid **b** 0.05 M  $\text{InCl}_3$ , 0.03 M  $\text{SbCl}_3$ , 0.30 M sodium citrate, 0.20 M citric acid **c** 0.05 M  $\text{InCl}_3$ , 0.04 M  $\text{SbCl}_3$ , 0.30 M sodium citrate, 0.20 M citric acid

dependent on the molar ratio of In and Sb ions in the electrochemical bath is a limitation of this method. This means that if the deposition continues for long periods, the bath may have to be replaced by a fresh one or its composition readjusted. Another limitation of this work is that films grown for more than 20 min start to peel off from the substrates. This puts an upper limit on the film thickness at around 0.6–0.8 micron.

The growth of spherical InSb particles in the presence of sodium citrate can be explained on the basis of free energy considerations and the nature of the complexing agent. Normally, the crystal growth of particles occurs in such a way that the free energy of the particles is lowered. This happens when the volume to surface area of the particle is large. Spherical particles have a larger volume to surface ratio compared to particles of other shapes like cylinders, cubes, elongated beads, flowers and flakes etc, and is therefore the preferred shape of growth, provided the growth occurs at a sufficiently low rate. Growth under nonequilibrium conditions, however, can lead to particles of various other shapes. Thus controlling the growth rate or inducing

nonisotropic growth, by means of additives, is a way of controlling the particle shape. In the case of the electrodeposition of InSb, the electrolyte seems to favour nonisotropic growth in the absence of sodium citrate, leading to clusters having the shape of cauliflowers. When sodium citrate is added to the bath in sufficient concentrations, the large number of citrate ions present in the solution, cover the surface of the nanoparticles and thus stabilize the high surface energy. The nanoparticles acquire a negative surface charge when the citrate ions cap the particles. This surface charge causes repulsion among the different nanoparticles preventing their fusion and possible anisotropic growth. Thus the capping and stabilization, by the citrate ions, results in the formation of spherical nanoparticles during the electrodeposition process.

#### 4.4 Raman studies

Figure 9 shows the Raman spectra of thin films grown on brass sheet substrates from baths of four different compositions. The Raman graph shows that annealed films grown from bath of composition of 0.05 M InCl<sub>3</sub> and 0.04 M SbCl<sub>3</sub> on brass substrate show clearly separate peaks of the transverse optical (TO) and longitudinal optical (LO) phonon modes of the InSb thin film at 178 and 189 cm<sup>-1</sup> respectively, with additional peaks appearing at 150 and 110 cm<sup>-1</sup> assigned to TO–TA and 2TA phonon modes, respectively. The TO and LO phonon modes of the deposited thin films match closely with the TO and LO peaks reported for InSb nano wires [50]. Raman micrographs of non-stoichiometric thin films show only TO–TA and 2TA phonon modes with less intense peaks of TO and LO. The presence of TO and LO phonon modes confirms that the deposited films are crystalline in nature.

#### 4.5 Electrical studies

The resistivity of the electrodeposited films was studied using the four probe method and the conductivity type of the films was studied by the hot probe technique. The electrical studies show that the indium rich thin films are p-type and antimony rich thin films are n-type in conductivity. Annealing the films at temperature 300 °C, for 1 h in vacuum, shows no change in the type of conductivity. The stoichiometric films grown on metal substrates with p type conductivity have a resistivity in the range 10–20 Ω cm (corresponding to a conductivity range 0.5–0.1 S cm<sup>-1</sup>). A comparison with the conductivities published for various polymer composites can be made. Reddy et al. have reported a conductivity of 1.28 S cm<sup>-1</sup> for their POT Ag composites [51] and for their SPAN-M polymers, Reddy et al. [52] have measured a conductivity of 1.5 S cm<sup>-1</sup>, both of which are better conductors than our p-type InSb

samples. Xu and Tan [53] have reported conductivities in the range 0.2–0.8 S cm<sup>-1</sup> in their carbon nanotube polypyrrole hybrid nanotubes, which are again slightly higher than for our samples. However, the conductivity in InSb is due to impurity levels (Sb vacancies or In interstitials) and cannot be compared with conduction mechanisms in polymers.

## 5 Conclusions

In conclusion, polycrystalline InSb thin films were grown on different substrates from baths of four different compositions using an applied potential of –1.3 V versus an AgCl ref electrode. The stoichiometry of the deposited InSb thin films is strongly dependent on the In/Sb ionic ratio in the electrochemical bath. The electrochemical bath for the growth of films with the best stoichiometry was made up of aqueous solutions of 0.05 M InCl<sub>3</sub>, 0.04 M SbCl<sub>3</sub>, 0.30 M C<sub>6</sub>H<sub>8</sub>O<sub>7</sub>·H<sub>2</sub>O and 0.20 M Na<sub>3</sub>C<sub>6</sub>H<sub>5</sub>O<sub>7</sub>·H<sub>2</sub>O. Raman studies show clearly separated peaks of the transverse optical (TO) and longitudinal optical (LO) phonon modes for the stoichiometric InSb thin film at 178 and 189 cm<sup>-1</sup> respectively. The XRD results show that the thin films grown on brass sheet substrates are single phase InSb without the presence of elemental In and Sb. Hot probe studies show that the p type films have resistivity in range 10–20 Ω cm.

**Acknowledgements** The authors are thankful to Mr. S.D. Sharma and Mr. Shiv Kumar, IIC, IIT Roorkee, India for providing the XRD and SEM/EDAX facilities. We are also grateful to IISc Bangalore, for providing the Raman facilities.

## References

1. R.K. Mangal, Y. Vijay, Bull. Mater. Sci. **30**, 117 (2007).
2. S. Singh, K. Lal, A.K. Shrivastava, K.N. Sood, R. Kishore, Indian J. Eng. Mater. Sci. **14**, 55 (2007)
3. J.T. Wimmers, R.M. Davis, C.A. Niblack, D.S. Smith, Proc. SPIE **930**, 125–138 (1988)
4. D.L. Rode, Phys. Rev. B **3**, 3287 (1971)
5. N.K. Udayashankar, H.L. Bhat, Bull. Mater. Sci. **24**, 445 (2001)
6. J. Heremans, D.L. Partin, C.M. Thrush, Semi Sci. Technol. **8**, 424 (1993)
7. T. Ashley, A.B. Dean, C.T. Elliott, G.J. Pryce, A.D. Johnson, H. Willis, Appl. Phys. Lett. **66**, 481 (1995)
8. M. Edirisooriya, T.D. Mishima, C.K. Gaspe, K. Bottoms, R.J. Hauenstein, M.B. Santos, J. Cryst. Growth **311**, 1972–1975 (2009)
9. H.D. Parka, S.M. Prokesa, M.E. Twigga, Y. Dingb, Z.L. Wangb, J. Cryst. Growth **304**, 399–401 (2007)
10. K. Togawa, H. Sanbonsugi, A. Sandhu, M. Abe, H. Narimatsu, K. Nishio, H. Handa, Jpn. J. Appl. Phys. **44**, 46–49 (2005)
11. A. Okamoto, T. Yoshida, S. Muramatsu, I. Shibasaki, J. Cryst. Growth **201**, 765 (1999)
12. M.K. Carpenter, M.W. Verbrugge, J. Mater. Res. **9**, 2584 (1984)
13. I. Kimukin, N. Biyikli, E. Ozbay, J. Appl. Phys. **94**, 8 (2003)

14. Y. Wang, J. Chi, K. Banerjee, D. Grutzmacher, T. Schapers, J.G. Lu, *J. Mater. Chem.* **21**, 2459–2462 (2011)
15. T. Miyazaki, S. Adachi, *Appl. Phys.* **70**, 1672 (1991)
16. D.G. Avery, D.W. Goodwin, A.E. Rennie, *J. Sci. Instrum.* **34** (1958)
17. C.K. Sumesh, K.D. Patel, G.K. Solanki, V.M. Pathak, R. Srivastava, *Eur. Phys. J. Appl. Phys.* **54**, 10303 (2011)
18. T. Miyazaki, M. Kunugi, Y. Kitamura, S. Adachi, *Thin Solid Films* **287**, 51–56 (1996)
19. M. Tomisu, N. Inoue, Y. Yasuoka, *Vacuum* **47**, 239–242 (1996)
20. K.R. Reddy, V.G. Gomes and M. Hassan, *Mat. Res. Express* **1**, 015012 (2014)
21. K.R. Reddy, K.P. Lee, A.I. Gopalan, *J. Appl. Polym. Sci.* **106**, 1181–1191 (2007)
22. A. Phuruangrat, S. Thongtemb, T. Thongtem, *Mater. Des.* **107**, 250–256 (2016)
23. K. Raghava, K. Nakata, T. Ochiai, T. Murakami, D. Tryk, *J. Nanosci. Nanotechnol.* **11**, 3692–3695 (2011)
24. M. Hassan, E. Haque, K.R. Reddy, A.I. Minett, J. Chenc, V.G. Gomes, *Nanoscale* **6**, 11988–11994 (2014)
25. K.R. Reddy, K.P. Lee, A.I. Gopalan, *Colloid. Surf. A* **320**, 49–56 (2008).
26. M. Cakici, R.R. Kakarla, F.A. Marroqui, *Chem. Eng. J.* **309**, 151–158 (2017)
27. A.M. Showkat, Y.P. Zhang, M.S. Kim, A.I. Gopalan, K.R. Reddy, K.P. Lee, *Bull. Korean Chem. Soc.* **28**, 1985 (2007)
28. K.R. Reddy, B.C. Sin, C.H. Yoo, W. Park, K.S. Ryu, J.S. Lee, D. Sohn, Y. Lee, *Scr. Mater.* **58**, 1010–1013 (2008)
29. K.R. Reddy, B.C. Sina, K.S. Ryua, J.C. Kimb, H. Chungc, Y. Leea, *Synth. Met.* **159**, 595–603 (2009)
30. K.R. Reddy, K.V. Karthik, S.B.B. Prasad, S.K. Soni, H.M. Jeong, A.V. Raghu, *Polyhedron* **120**, 169–174 (2016)
31. J. Ortega, H. Herrero, *J. Electrochem. Soc.* **136**, 3388 (1989)
32. J. Machesney, J. Haigh, I.M. Dharmadasa, D.J. Mowthorpe, *Opt. Mater.* **6**, 63 (1996)
33. V.M. Kozlov, V. Agrigento, D. Bontempi, S. Canegallo, C. Manitou, A. Toussimi, *J. Alloys Comp.* **259**, 234 (1997)
34. T. Fulop, C. Bekele, U. Landau, J. Angus, K. Kash, *Thin Solid Films* **449**, 1–5 (2004)
35. M.I. Khan, X. Wang, X. Jing, K.N. Bozhilov, C.S. Ozkan, *J. Nanosci. Nanotechnol.* **8**, 1–6 (2008)
36. K.E. Hnida, L. Akinsinde, J. Gooth, K. Nielsch, R.P. Socha, A. Łaszcz, A. Czerwinski, G.D. Sulka, *Nanotechnology* **26**, 285701 (2015)
37. S.R. Das, C. Akatay, A. Mohammad, M.R. Khan, K. Maeda, R.S. Deacon, K. Ishibashi, Y.P. Chen, T.D. Sands, M.A. Alam, D.B. Janes, *J. App. Phys.* **116**, 083506 (2014)
38. K.E. Hnida, J. Mech, K. Szaciłowski, R.P. Socha, M. Gajewska, K. Nielsch, M. Przybylski, G.D. Sulkag, *J. Mater. Chem. C* **4**, 1345 (2016)
39. Y.T. Hsieh, Y.C. Chen, I.W. Sun, *Chem. Electro. Chem.* **3**, 638–643 (2016).
40. S.O. Pagotto, M. Ballester, *Surf. Coat. Technol.* **122**, 10–13 (1999)
41. M.S. Chandrasekhar, M. Pushpavanam, *Electrochim. Acta* **53**, 3313–3322 (2008)
42. D. Grujicic, B. Pesic, *Electrochim. Acta* **47**, 2901–2912 (2002)
43. L. Zhou, Y. Dai, H. Zhang, Y. Jia, J. Zhang, C. Li, *Bull. Korean Chem. Soc.* **33**, 1541 (2012)
44. S.K.J. Al-Ani, Y.N. Obaid, S.J. Kasim, M.A. Mahdi, *Int. J. Nanoelectron. Mater.* **2**, 99–109 (2009)
45. Y. Yang, L. Li, X. Huang, G. Li, L. Zhang, *J. Mater. Sci.* **42**, 2753–2757 (2007)
46. B. Williamson, R.C. Smallman, *Philos. Mag.* **1**, 34 (1956)
47. A. Salem, S.S. Ahmed, S.N. Alamri, *Indian J. Pure Appl. Phys.* **53**, 696–700 (2015)
48. M.A. Islam, K.S. Rahman, F. Haque, M. Akhtaruzzaman, M.M. Alam, Z.A. Alothman, K. Sopian, N. Amin, *Chalcogenide Lett.* **11**, 233–239 (2014)
49. V. Senthilkumar, S. Venkatachalam, C. Viswanathan, S. Gopal, S.K. Narayandass, D. Mangalaraj, K.C. Wilson, K.P. Vijayakumar, *Cryst. Res. Technol.* **40**, 573–578 (2005)
50. X. Zhang, Y. Hao, G. Meng, L. Zhang, *J. Electrochem. Soc.* **152**, 664–668 (2005)
51. K.R. Reddy, K.P. Lee, Y. Lee, A.I. Gopalan, *Mater. Lett.* **62**, 1815–1818 (2008)
52. K.R. Reddy, K.P. Lee, A.I. Gopalan, M.S. Kim, A.M. Showkat, Y.C. Nho, *Polym. Chem.* **44**, 3355–3364 (2006)
53. H.X. Tan, X.C. Xu, *RSC Adv.* **5**, 61383–61389 (2015)